2022-12-01

Two-Step Single Qubit Gates For Superconducting Qubits

Edward Takyi
University of Texas at El Paso

TWO-STEP SINGLE QUBIT GATES FOR SUPERCONDUCTING QUBITS

EDWARD TAKYI

Master's Program in Physics

APPROVED:

Yun-Pil Shim, Ph.D., Chair

Ramon Ravelo, Ph.D.

Rajendra Zope, Ph.D.

Vladik Kreinovich, Ph.D.

Stephen L. Crites, Ph.D.
Dean of the Graduate School

TWO-STEP SINGLE QUBIT GATES FOR SUPERCONDUCTING QUBITS

by

EDWARD TAKYI, B.Sc.

THESIS

Presented to the Faculty of the Graduate School of

The University of Texas at El Paso

in Partial Fulfillment

of the Requirements

for the Degree of

MASTER OF SCIENCE

Department of Physics

THE UNIVERSITY OF TEXAS AT EL PASO

December 2022

Table of Contents

List of Figures

Acknowledgments

My most profound appreciation goes to my supervisor, Dr. Yun-Pil Shim who gave me the opportunity and provided me with invaluable guidance throughout this research. Without his guidance and persistent help, this thesis would not have been possible. Dr. Shim's unassuming approach to research and science is a source of inspiration. I could not have imagined having a better supervisor and mentor for my MS study period.

Very special thanks to my committee members, Dr. Rajendra Zope, Dr. Ramon Ravelo, and Dr. Vladik Kreinovich for their patience with me and their dedication to this work.

I must confess that it has been an amazing experience working with my research group members, Dr. Omadillo Abduzarakov and Miguel Rodriguez. Dr. Omadillo has a unique way of keeping me in the right situations to spark growth academically and personally. I am appreciative of the countless insightful conversations I had with Miguel as well.

Also, I am heartily thankful to my affectionate siblings who keep me motivated, remind me of what is important in life, and are always supportive of my adventures. Finally, I wish to express my tenderest gratitude to my dear parents whose constant love and support keep me motivated and optimistic.

Abstract

Why quantum information processing? Contemporary manipulation and transmission of information is executed through physical machines (computers, routers, scanners, etc.) in which Classical Mechanics is used to describe the embodiment and transformation of information. However, the physical theory of the world is not Classical Mechanics. And so, there is no reason to suppose that machines following the laws of Classical Mechanics would have the same computational power like quantum machines. Quantum computers would break the rules of classical computers and they would be able solve problems that are intractable on conventional supercomputers.

In order to fabricate quantum computers and make significant strides in the field of quantum data, we need quantum objects that can function as qubits. A qubit is the quantum mechanical analogue of a classical bit. To implement qubits, numerous techniques have been put forth, most of which rely on microscopic quantum systems like nuclear or electronic spins, photon polarizations, or electronic levels in trapped ions or crystal defects. However, one method uses the macroscale quantum phenomenon known as superconductivity. This has two significant benefits. Firstly, these systems can be constructed to meet desired criteria, unlike an atom, which is fixed by nature. Secondly, their size makes it possible to construct them using the scalable, well-known micro-fabrication techniques used in the traditional semiconductor industry, which is crucial if these qubits are to be produced into arbitrarily large computers. Currently, superconducting qubits are the leading candidates for qubit architecture due to their relative ease of fabrication and long coherence times.

From the mathematical viewpoint, every single-qubit gate (up to a global phase) is a rotation in the Bloch sphere representation. In practice, we cannot directly implement rotations around all possible axes. However, it is practically possible to implement rotations around fixed axes from coordinate planes, i.e., xy-, xz-, and yz-planes. At present, single qubit gates are implemented as a composition of three sequential rotations around fixed axes

from coordinate planes. In this thesis, we demonstrate that for any coordinate plane, any single-qubit gate (up to a global phase) can be implemented as a composition of only two sequential rotations around arbitrary axes that have been constrained to lie in that single plane. This reduction from three to two implementable rotations makes qubit processing faster and more reliable. Our technique is readily applicable to many qubit systems especially, superconducting qubit systems.

Chapter 1

Introduction

1.1 Objectives

According to the quantum circuit model [1], a universal quantum computer requires an entangling two-qubit gate such as CNOT, and a set of single-qubit gates [2]. It is therefore important to be able to perform gate operations as efficiently as possible in order to minimize the effects of decoherence or gating errors. Although a finite set of quantum gates is sufficient for universality, fault-tolerant circuits require a large number of gates, even for very simple operations [3]. Any quantum gate or single-qubit unitary operation can be viewed as a rotation. Single-qubit gates are typically experimentally implemented using two or three fixed rotation axes and up to three rotation steps. In this work, we demonstrate that two sequential rotation steps are enough to create a single-qubit gate if the two rotation axes are fixed in a single plane. This work was primarily motivated by superconducting qubits. Superconducting qubits are of interest because they are created in decoherence-free subspaces and subsystems.

1.2 Classical Bits

A binary number is a number that has been number expressed in the base -2 numeral system, a numeral system that uses only 2 numbers; specifically, “0” zero and “1” one. Each digit is referred to as a bit. Due to its straightforward implementation in digital electronic circuitry, using logic gates, the binary system is used by all classical computers as a preferred system of use. A bit is the smallest unit of information in a digital computer. Digital computers

store and process information using bits. The bits are represented by the absence or presence of an electrical signal, encoding "0" and "1" respectively. A bit can have a value of either true or false, on or off, etc.

In a digital computer, we can represent information using character codes, where alpha-numeric characters and other symbols are represented using decimal numbers. These decimal numbers are in turn expressed in binary notation as a sum of increasing powers of two,

$$b_n \cdot 2^n + \ldots + b_2 \cdot 2^2 + b_1 \cdot 2^1 + b_0 \cdot 2^0,$$

where $b_n, \ldots b_2, b_1, b_0$ are the binary digits called "bits" with values 0 or 1.

$$b_i \in \{0, 1\}.$$

Hence in classical computing, information is represented using bits, which are a string of 0's and 1's.

For example, 2 bits can represent the numbers $0 - 3$:

$$0 = 0 \cdot 2^1 + 0 \cdot 2^0 = 0 \tag{1.1}$$

$$1 = 0 \cdot 2^1 + 1 \cdot 2^0 = 01 \tag{1.2}$$

$$2 = 1 \cdot 2^1 + 0 \cdot 2^0 = 10 \tag{1.3}$$

$$3 = 1 \cdot 2^1 + 1 \cdot 2^0 = 11 \tag{1.4}$$

1.3 Quantum Bits

The quantum equivalent of a classical bit is a quantum bit (qubit), a basic quantum information unit. A quantum bit is a 2-state quantum mechanical system, one of the most basic quantum systems that exhibits the peculiarities of Quantum Mechanics. In classical computing, 0, and 1 are represented by a binary state, e.g., the voltage on or off or the absence or presence of electrical charge. However, in a quantum computer, 0's and 1's are

represented by two quantum states that differ in some quantum number. Quantum computers encode information using qubits. Equivalently, 0 and 1 are represented by two different eigenstates of some quantum operator. Unlike classics computing, a quantum state can exist as a superposition of the two quantum states, i.e., a superposition of 0 and 1 is possible. For example,

- A qubit could be a superposition of up and down alignment of an electron spin.
- Electron in the ground state or the excited state of a trapped ion or an electron orbiting the nucleus of an atom.
- Photon with horizontal (H) or vertical (V) polarization.
- Photon with $+45^\circ$ or -45° polarization.
- Photon with left circular polarization (LCP) or right circular polarization (RCP).
- Superconducting current flowing clockwise or counterclockwise.

In classical computer technologies, a processed bit is implemented by one of two levels of low DC voltage. To switch from one level of electrical voltage to another, a so-called "forbidden" zone must be passed as fast as possible because electrical voltage cannot simultaneously change from one level to another. According to Quantum Mechanics, a qubit's general state can be a coherent superposition of both 0 and 1, but a bit can only have one of these states [4]. As a result, one qubit can entirely encode one bit. However, a qubit can store up to two or more bits of information.

1.4 Dirac Notation

The essence of Dirac notation is that the state of a quantum system is fully described by a vector in an associated Hilbert space. In quantum theory, an object enclosed using the Dirac

notation $|\ \rangle$ is called a ket vector, e.g. $|\psi\rangle$. An object enclosed using the Dirac notation $\langle|$ is called a bra vector, e.g. $\langle\phi|$. Any ket can be written as

$$|\psi\rangle = \sum_i a_i |i\rangle$$

where

$$\langle i \mid \psi\rangle = a_i$$

The corresponding bra vector can be written as

$$\langle\psi| = \sum_i a_i \langle i|$$

where

$$\langle\psi|\, i\rangle = a_i^*$$

Dirac's notation is a convenient way of representing quantum states and their superpositions. A qubit can be encoded by preparing an atom in the ground state,

$$|\text{ground state}\rangle$$

or the excited state,

$$|\text{excited state}\rangle.$$

Spin states of an electron (used as qubits) can be represented as

$$|z_+\rangle\,, |z_-\rangle \ \text{ or } |\uparrow\rangle, |\downarrow\rangle$$

Photon polarization states (used as qubits) can be represented as

$$|H\rangle\,, |V\rangle \ \text{ or } |+45^\circ\rangle, |-45^\circ\rangle \text{ or } |LCP\rangle, |RCP\rangle$$

The above states can be generalized to the $|0\rangle$, and $|1\rangle$ basis states. That is, one state represents $|0\rangle$ and the other state represents $|1\rangle$. Actually, any pair of vectors $|\phi\rangle, |\psi\rangle \in \mathbb{C}^2$ that are linearly independent could serve as a basis. The basis states are orthonormal [5] :

$$\langle 0 \mid 0\rangle = \langle 1 \mid 1\rangle = 1, \text{ and } \langle 0 \mid 1\rangle = \langle 1 \mid 0\rangle = 0.$$

In quantum computing, most of the time, the basis states $|0\rangle$ and $|1\rangle$ are used. They are called single-qubit computational (or standard) basis sates.

1.5 Qubit States

A qubit is in its pure state when the basis states are coherently superimposed. This means that a linear combination of $|0\rangle$ and $|1\rangle$ clearly describes a single qubit :

$$|\psi\rangle = \alpha|0\rangle + \beta|1\rangle,$$

where $|\alpha\rangle$ and $|\beta\rangle$ are the complex numbers that represent the probability amplitudes. When measuring this qubit in the standard basis, Born rule states that the likelihood of outcome $|0\rangle$ with the value "0" would be $|\alpha|^2$ and the likelihood of outcome $|1\rangle$ would with the value "1" would be $|\beta|^2$ [6].

The second axiom of probability theory states that $|\alpha|$ and $|\beta|$ must be constrained by the equation : $|\alpha|^2+|\beta|^2 = 1$. This is because the absolute squares of the amplitudes (α and β) equate to probability. The two computational basis states which consist of the two orthonormal basis states, $\{|0\rangle, |1\rangle\}$, make up the two-dimensional linear vector space (Hilbert space) of the qubit. Accordingly, product basis states can be created by combining qubit's states. A collection of qubits is called a quantum register. For two qubits we can write

$$|\psi\rangle = |\psi_1\rangle \otimes |\psi_2\rangle = \underbrace{(\alpha_1|0\rangle_1 + \beta_1|1\rangle_1)}_{\text{qubit 1}} \otimes \underbrace{((\alpha_2|0\rangle_2 + \beta_2|1\rangle_2)}_{\text{qubit 2}}$$

Expanding this two-qubit state gives

$$|\psi\rangle = \alpha_1\alpha_2|0\rangle_1|0\rangle_2 + \alpha_1\beta_2|0\rangle_1|1\rangle_2 + \beta_1\alpha_2|1\rangle_1|0\rangle_2 + \beta_1\beta_2|1\rangle_1|1\rangle_2$$

$$|\psi\rangle = \alpha_{00}|00\rangle + \alpha_{01}|01\rangle + \alpha_{10}|10\rangle + \alpha_{11}|11\rangle$$

Here, the expression has been simplified by abandoning the particle subscripts and compacting the ket notation so that for example, $|0\rangle_1, |0\rangle_2$ is written $|00\rangle$. The states $|00\rangle$, $|01\rangle$, $|10\rangle$, and $|11\rangle$ form an orthonormal basis for two qubits.

So far, we have seen that there are 2 computational basis for single-qubits: $|0\rangle, |1\rangle$. There are 4 computational basis states for a two-qubit system: $|00\rangle, |01\rangle, |10\rangle, |11\rangle$. And there would be 2^N computational basis states for a multi-qubit system of N qubits: $|00...00\rangle$, $|00...01\rangle$, $|00...10\rangle$ ... $|11...11\rangle$

1.6 The Bloch Sphere

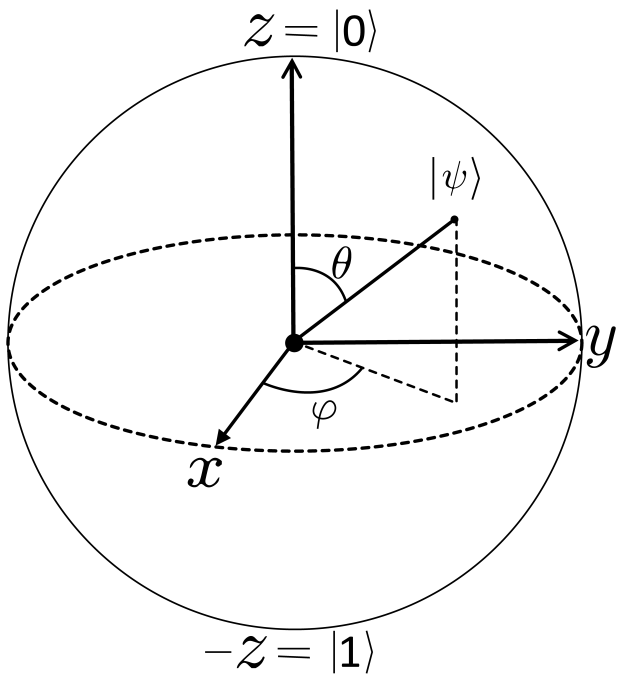

Figure 1.6.1: The Bloch Sphere https://tinyurl.com/5n76jr5u

Operations on single qubits commonly used in quantum computing can be represented on the Bloch sphere. Pure single-qubit states are geometrically depicted as a point on the Bloch sphere [4]. The North Pole and the South Pole typically represent the orthonormal computational basis states $|0\rangle$ and $|1\rangle$, respectively, and these might correspond to the spin-up or spin-down states of an electron. Any arbitrary single qubit pure state, up to a global phase, is represented by a point on the unit sphere (Bloch Sphere). This relates the superposition of the basis states to the angular coordinates of the point. Any unitary operation, taking an initial state to the final state of a single-qubit, is equivalent to a composition of one or more simple rotations on the Bloch sphere. The Bloch Sphere picture is exquisite and powerful for single qubits because it helps us to visualize the superposition of quantum states in terms of the angular coordinates. The Bloch sphere picture also helps us to visualize the unitary operations on quantum states as rotations on the sphere. It provides an intuitive picture

of what is going on when we apply a single qubit gate to a two-level quantum system such as a qubit. Given the computational orthonormal basis, any pure state $|\psi\rangle$ of a two-level quantum system can be written as a superposition of the basis vectors $|0\rangle$ and $|1\rangle$, where the coefficients of each of the two basis vectors is a complex number. This implies that the state is described by four real numbers. But only the relative phase of the coefficients of the two basis vectors has any physical meaning. The global phase of the quantum system is not directly measurable. The coefficient of $|0\rangle$ is taken to be real and non-negative. This allows the quantum state to be described by only three real numbers, giving rise to the three dimensions of the Bloch Sphere. We know from Quantum Mechanics that the probability of the system has to be one

$$\langle \psi \mid \psi \rangle = 1 \text{ or } \|\psi\|^2 = 1$$

Given these constraints, the formal equation for declaring qubit's state is

$$|\psi\rangle = \cos\left(\frac{\theta}{2}\right)|0\rangle + e^{i\phi}\sin\left(\frac{\theta}{2}\right)|1\rangle,$$

where $0 \leqslant \theta \leqslant \pi$ and $0 \leqslant \phi \leqslant 2\pi$. Since the Bloch sphere is well, a sphere, and since all pure qubits are just points on the surface of the sphere, it is convenient to represent qubits in spherical coordinates (r, θ, ϕ). The radius will always be 1. So, to fully specify the state of a qubit, we only need to specify the two angles (θ and ϕ) as shown in the Bloch Sphere diagram above. To describe the orientation of a qubit in three-dimensional space,

1. The polar angle θ represents the angle from the positive z-axis (the $|0\rangle$ state) to the positive x-axis on the x-z plane. This polar angle tells how much of 1 and 0 there is in the qubit

2. The azimuthal angle ϕ, describes the angle from the positive x-axis (the $|+\rangle$ state) to the positive y-axis on the x-y plane. The azimuthal angle specifies the relative phase between the states 0 and 1.

The representation is always unique because even though the value of ϕ is not unique, when $|\psi\rangle$ is one of the states $|0\rangle$ or $|1\rangle$, the point represented by θ and ϕ is unique.

Chapter 2

Quantum Gates

A gate can be thought of as an abstraction representing information processing. In classical computers, bits are processed using classical logic gates. However, in quantum computers, qubits (information) are processed using quantum logic gates. Quantum logic gates are unitary operations and can be represented by matrices. Any unitary operation, taking an initial state to the final state of the single-qubit, is equivalent to a composition of one or more simple rotations on the Bloch sphere [4]. A quantum gate with n inputs and outputs can be represented by an n by n matrix.

Qubits can of course assume the classical states $|0\rangle$ and $|1\rangle$ at the north pole and south pole of the Bloch sphere respectively, but they can also assume arbitrary superpositions of $|0\rangle$ and $|1\rangle$, corresponding to any other position on the sphere. Single-qubit gate operations translate an arbitrary quantum state from one point on the Bloch sphere to another point by rotating the Bloch vector (spin) a certain angle about a particular axis. 2 by 2 unitary matrices are used to represent single qubit gates.

There are also multi-qubit quantum logic gates like two-qubit gates or three-qubit gates. Two-qubit gates are often "conditional" gates and they take two qubits as inputs. Typically, the first qubit is the "control" qubit, and the second is the "target" qubit. A unitary operator is applied to the target qubit, dependent on the state of the control qubit. Two qubit gates are represented by 4 by 4 matrices

To implement any quantum logic, a universal set of single-qubit and two-qubit gates is sufficient. This means that a gate set of two-qubit and single qubit gates can in principle, reach "any" state in the multi-qubit state space. We also note that each of the single-qubit and two-qubit gates is reversible, that is, given the output state, one can uniquely determine

the input state. In this study, we considered only single qubit gates.

2.1 The Identity Gate

The Identity gate is a single-qubit operation that leaves the computational basis states unchanged.

$$I = \begin{pmatrix} 1 & 0 \\ 0 & 1 \end{pmatrix}$$

The identity gate does no operation; applying the identity gate anywhere in a circuit has no effect on the qubit state. For simulations, this gate is useful in combination with the error model instruction.

Because it represents no specific action on a qubit (do nothing), the depolarizing error model will take this gate into account when distributing errors on the qubits. This can be used as a simple version of the decoherence of the qubit.

2.2 The Pauli X Gate

The Pauli X gate and the classical NOT gate are analogous

$$X = U_{\text{NOT}} = \begin{pmatrix} 0 & 1 \\ 1 & 0 \end{pmatrix}$$

$$U_{\text{NOT}} |0\rangle = \begin{pmatrix} 0 & 1 \\ 1 & 0 \end{pmatrix} \begin{pmatrix} 1 \\ 0 \end{pmatrix} = \begin{pmatrix} 0 \\ 1 \end{pmatrix}$$

$$U_{\text{NOT}} |1\rangle = \begin{pmatrix} 0 & 1 \\ 1 & 0 \end{pmatrix} \begin{pmatrix} 0 \\ 1 \end{pmatrix} = \begin{pmatrix} 0 \\ 1 \end{pmatrix}$$

The X-gate performs a half-turn in the Bloch sphere about the x-axis.

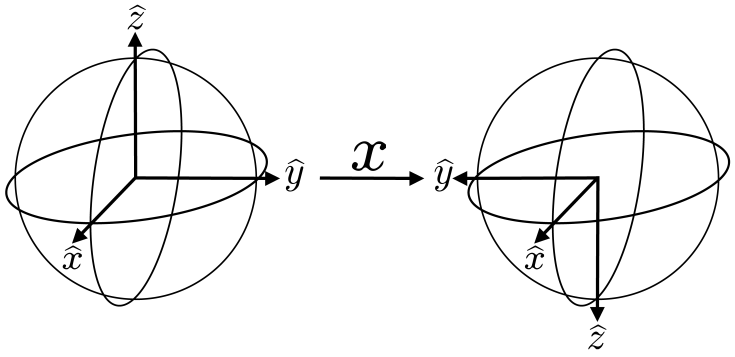

Figure 2.2.1: Rotation around the x-axis

2.3 The Pauli Y-gate

$$Y = \begin{pmatrix} 0 & -i \\ i & 0 \end{pmatrix} = -i|0\rangle\langle 1| + i|1\rangle\langle 0|$$

$$Y|0\rangle = \begin{pmatrix} 0 & -i \\ i & 0 \end{pmatrix} \begin{pmatrix} 1 \\ 0 \end{pmatrix} = \begin{pmatrix} 0 \\ i \end{pmatrix} = i|1\rangle$$

$$Y|1\rangle = \begin{pmatrix} 0 & -i \\ i & 0 \end{pmatrix} \begin{pmatrix} 0 \\ 1 \end{pmatrix} = \begin{pmatrix} -i \\ 0 \end{pmatrix} = -i|0\rangle$$

With respect to the computational basis, we interchange the zero and one states and apply a relative phase flip.

We can think of the Pauli Y-gate as rotating by π radians around the y-axis of the Bloch Sphere. This is because the Y-gate implements a half-turn in the Bloch sphere about the $\widehat{y}$-axis. The Pauli Y-gate can also be considered as a combination of X and Z gates, $Y = -iZX$

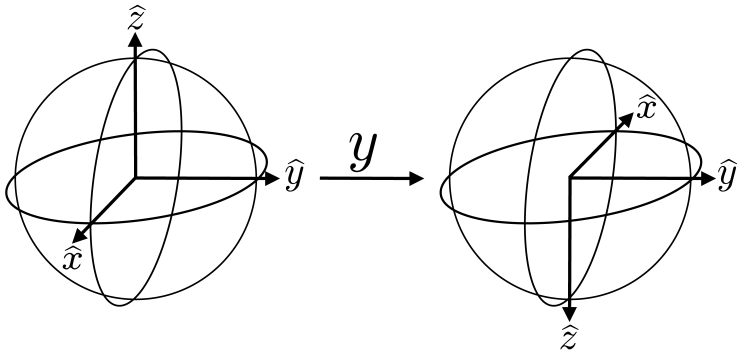

Figure 2.3.1: Rotation around the y-axes

2.4 The Pauli Z-gate

The Pauli Z gate is represented by

$$Z = \begin{pmatrix} 1 & 0 \\ 0 & -1 \end{pmatrix} = |0\rangle\langle 0| - |1\rangle\langle 1|$$

$$Z|0\rangle = \begin{pmatrix} 1 & 0 \\ 0 & -1 \end{pmatrix} \begin{pmatrix} 1 \\ 0 \end{pmatrix} = \begin{pmatrix} 1 \\ 0 \end{pmatrix} = |0\rangle$$

$$Z|1\rangle = \begin{pmatrix} 1 & 0 \\ 0 & -1 \end{pmatrix} \begin{pmatrix} 0 \\ 1 \end{pmatrix} = \begin{pmatrix} 0 \\ -1 \end{pmatrix} = -|1\rangle$$

The Pauli Z gate performs a π radians rotation around the z-axis of the Bloch sphere.

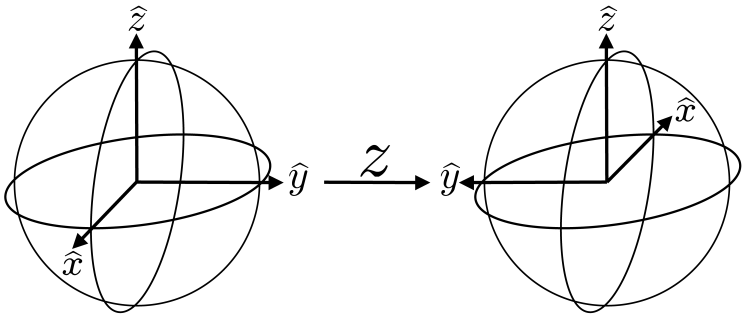

Figure 2.4.1: Rotation around the z-axes

2.5 The Hadamard Gate

The Hadamard gate is given by the matrix below:

$$H \doteq \frac{1}{\sqrt{2}} \begin{pmatrix} 1 & 1 \\ 1 & -1 \end{pmatrix}$$

The Hadamard operator acting on $|0\rangle$ is given by:

$$H|0\rangle = \frac{1}{\sqrt{2}}(|0\rangle\langle 0| + |0\rangle\langle 1| + |1\rangle\langle 0| - |1\rangle\langle 1|)|0\rangle = \frac{|0\rangle + |1\rangle}{\sqrt{2}} = |+\rangle$$

Similarly we find that

$$H|1\rangle = \frac{|0\rangle - |1\rangle}{\sqrt{2}} = |-\rangle$$

These two basis states,

$$|+\rangle, |-\rangle$$

are called the x-basis states. They are orthonormal.

2.6 The Phase Gate

The Phase gate has a matrix form given by

$$P = \begin{pmatrix} 1 & 0 \\ 0 & e^{i\theta} \end{pmatrix}$$

The P-gate performs a rotation of θ around the z-axis direction. This gate shifts or alters the relative phase of the amplitudes α and β of a qubit. The P-gate needs a number ϕ to tell it exactly what to do.

The Z gate is just the special case where $\phi = \pi$, and hence $e^{i\pi} = -1$. In general, the action of the phase shift gate on a qubit is

$$P\psi = P = \begin{pmatrix} 1 & 0 \\ 0 & e^{i\phi} \end{pmatrix} \begin{pmatrix} \alpha \\ \beta \end{pmatrix} = \begin{pmatrix} \alpha \\ e^{i\phi}\beta \end{pmatrix}$$

Given a qubit

$$|\psi\rangle = \cos\theta|0\rangle + e^{i\phi}\cos\theta|1\rangle, \tag{2.1}$$

in terms of outer product notation, the phase shift operator (using an angle γ) can be written as:

$$P = |0\rangle\langle 0| + e^{i\gamma}|1\rangle\langle 1|$$

So

$$P|\psi\rangle = cos\phi|0\rangle + e^{i(\gamma+\phi)}|1\rangle.$$

We see that the phase shift operator takes the azimuthal angle ϕ to $\phi + \gamma$.

We have seen that the Z gate is a special case of the phase shift operator where we take the angle to be π. There are other special cases of interest.

2.6.1 The S Gate

The S gate is a special case of the Phase shift gate when we take $\theta = \pi/2$. By Euler's identity, $e^{\pi/2} = \cos(\pi/2) + i\sin(\pi/2) = i$. The S gate has the matrix representation in the standard or computational basis given by

$$S = \begin{pmatrix} e^{-i\pi/2} & 0 \\ 0 & e^{i\pi/2} \end{pmatrix}$$

2.6.2 The T Gate

$$T = e^{i\pi/8}\begin{pmatrix} e^{-i\pi/8} & 0 \\ 0 & e^{i\pi/8} \end{pmatrix}, \tag{2.2}$$

i.e.,

$$T = e^{i\pi/8}\begin{pmatrix} e^{-i\pi/8} & 0 \\ 0 & e^{i\pi/8} \end{pmatrix} = e^{i\pi/8}e^{-i\pi Z/8} = e^{i\pi/8}R_z\left(\frac{\pi}{4}\right).$$

This shows us that the T gate is equivalent to a 45 degree rotation around the z-axis.

2.7 Single-Qubit Gates: Rotations Around Axes

2.7.1 R_x gate

Rotate θ radians counter-clockwise about the x-axis of the Bloch sphere.

$$R_x(\theta) = e^{-i\frac{1}{2}\theta X} = \cos\left(\frac{1}{2}\theta\right) I - i\sin\left(\frac{1}{2}\theta\right) X = \begin{pmatrix} \cos\left(\frac{1}{2}\theta\right) & -i\sin\left(\frac{1}{2}\theta\right) \\ -i\sin\left(\frac{1}{2}\theta\right) & \cos\left(\frac{1}{2}\theta\right) \end{pmatrix} \tag{2.3}$$

2.7.2 R_y Gate

This gate is described in [7]. Rotate θ radians anti-clockwise about the $\widehat{y}$ axis of the Bloch sphere.

$$R_y(\theta) = e^{-i\frac{1}{2}\theta Y} = \cos\left(\frac{1}{2}\theta\right) I - i\sin\left(\frac{1}{2}\theta\right) Y = \begin{pmatrix} \cos\left(\frac{1}{2}\theta\right) & -\sin\left(\frac{1}{2}\theta\right) \\ \sin\left(\frac{1}{2}\theta\right) & \cos\left(\frac{1}{2}\theta\right) \end{pmatrix} \tag{2.4}$$

2.7.3 R_z Gate

Rotate θ radians counter-clockwise about the z-axis of the Bloch sphere. Refer figure 2.7.1

$$R_z(\theta) = e^{-i\frac{1}{2}\theta Z} = \cos\left(\frac{1}{2}\theta\right) I - i\sin\left(\frac{1}{2}\theta\right) Z = \begin{bmatrix} e^{-i\frac{1}{2}\theta} & 0 \\ 0 & e^{+i\frac{1}{2}\theta} \end{bmatrix} \tag{2.5}$$

2.7.4 $R_{\vec{n}}$ Gate

A rotation of θ radians anti-clockwise about an arbitrary axis in the Bloch sphere.

$$R_{\vec{n}}(\theta) = e^{-i\frac{1}{2}\theta(n_x X + n_y Y + n_z Z)} = \cos\left(\frac{1}{2}\theta\right) I - i\sin\left(\frac{1}{2}\theta(n_x X + n_y Y + n_z Z)\right)$$

$$= \begin{bmatrix} \cos\left(\frac{1}{2}\theta\right) - in_z\sin\left(\frac{1}{2}\theta\right) & -n_y\sin\left(\frac{1}{2}\theta\right) - in_x\sin\left(\frac{1}{2}\theta\right) \\ n_y\sin\left(\frac{1}{2}\theta\right) - in_x\sin\left(\frac{1}{2}\theta\right) & \cos\left(\frac{1}{2}\theta\right) + in_z\sin\left(\frac{1}{2}\theta\right) \end{bmatrix} \tag{2.6}$$

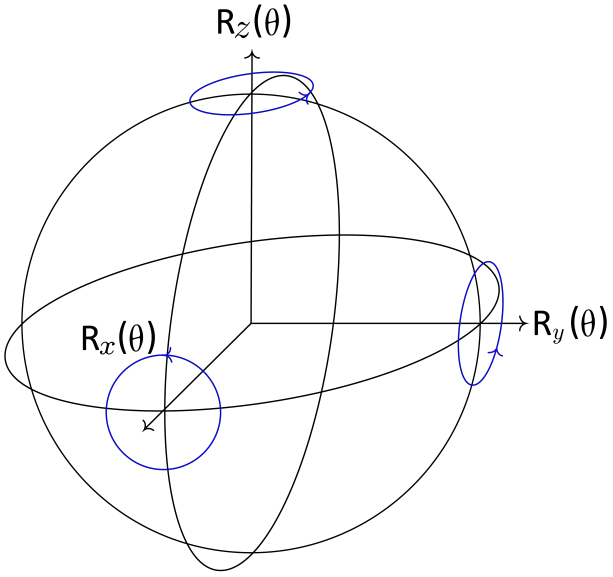

Figure 2.7.1: Pauli rotations of the Bloch Sphere

Every single-qubit gate can be represented as a rotation (up to phase) with some values (n_x, n_y, n_z, θ), where $n_x^2 + n_y^2 + n_z^2 = 1$ and θ runs between π and $-\pi$. The Pauli gates are the rotations around the principal axes.

$$\begin{aligned} R_x(\theta) &= R_{\vec{n}}(\theta), \quad \vec{n} = (1,0,0) \\ R_y(\theta) &= R_{\vec{n}}(\theta), \quad \vec{n} = (0,1,0) \\ R_z(\theta) &= R_{\vec{n}}(\theta), \quad \vec{n} = (0,0,1) \end{aligned} \tag{2.7}$$

By exponentiating a given matrix, we can come up with more gates. In fact we can create rotation operators to represent rotation about the x, y, and z axes on the Bloch sphere by

exponentiating the Pauli matrices. These are given by

$$\begin{aligned}
\widehat{R}_x(\theta) = \exp\left(-i\frac{\theta}{2}\widehat{\sigma}_x\right) &= \begin{pmatrix} \cos\frac{\theta}{2} & -i\sin\frac{\theta}{2} \\ -i\sin\frac{\theta}{2} & \cos\frac{\theta}{2} \end{pmatrix} \\
\widehat{R}_y(\theta) = \exp\left(-i\frac{\theta}{2}\widehat{\sigma}_y\right) &= \begin{pmatrix} \cos\frac{\theta}{2} & -\sin\frac{\theta}{2} \\ \sin\frac{\theta}{2} & \cos\frac{\theta}{2} \end{pmatrix} \\
\widehat{R}_z(\theta) = \exp\left(-i\frac{\theta}{2}\widehat{\sigma}_z\right) &= \begin{pmatrix} \exp\left(-i\frac{\theta}{2}\right) & 0 \\ 0 & \exp\left(i\frac{\theta}{2}\right) \end{pmatrix} \\
\widehat{R}_x(\pi) = -iX, \quad \widehat{R}_y(\pi) &= -iY, \quad \widehat{R}_z(\pi) = -iZ
\end{aligned} \tag{2.8}$$

$$\widehat{R}_{\hat{n}}(\theta) = \exp\left(-i\frac{\theta}{2}\widehat{\mathbf{n}}\cdot\overrightarrow{\boldsymbol{\sigma}}\right) = \cos\frac{\theta}{2}I - i\sin\frac{\theta}{2}\widehat{\mathbf{n}}\cdot\overrightarrow{\boldsymbol{\sigma}} = e^{i\alpha}\widehat{R}_z(\beta)\widehat{R}_y(\gamma)\widehat{R}_z(\delta) \tag{2.9}$$

e.g.:

$$H = \frac{1}{\sqrt{2}}\begin{pmatrix} 1 & 1 \\ 1 & -1 \end{pmatrix} = \widehat{R}_z(\pi)\widehat{R}_x\left(\frac{\pi}{2}\right)\widehat{R}_z(\pi) = i\widehat{R}_y\left(\frac{\pi}{2}\right)\widehat{R}_z(\pi).$$

2.8 Superconductivity

At "normal" temperatures, all materials have some amount of electrical resistance. This means they resist the flow of electricity in the same way a narrow pipe resists the flow of water. Due to resistance, some energy is lost as heat when electrons move through the electronics in our devices, like computers or cell phones. For most materials, this resistance remains even if the material is cooled to very low temperatures. Superconducting materials are an exception to this.

Below a certain critical temperature, superconducting materials undergo a transition into the superconducting state, characterized by two basic properties: firstly, they offer no resistance to the passage of electrical current. Since resistance falls to zero, current can circulate inside superconducting materials without any dissipation of energy. For instance, an electric current through a loop of superconducting wire such as Nb_3Sn or $NbTi$ can

persist indefinitely with no power source [8]. Secondly, provided they are sufficiently weak, external magnetic fields would not penetrate a superconductor but remain at its surface. This phenomenon is known as the Meisner effect.

Thus, superconductivity is a set of physical properties observed in certain materials where electrical resistance vanishes and magnetic flux fields are expelled from a material when the temperature of that material is below the critical temperature. Some prominent examples of superconducting materials are Al, Nb, $MgBr_2$, cuprates such as $YBa_2Cu_3O_7$, $Bi_2Sr_2Ca_2Cu_2O_8$ and iron pnictides such as $SmFeAsO$

2.9 Superconducting Qubits

In this section, we present a brief overview of superconducting qubits. The key to performing quantum coherent processing is the control of individual quantum degrees of freedom and their interactions. This makes it possible to carry out specific computing operations and quantum simulations that are not possible with current supercomputers. [4], [9]. Even after researchers have made significant theoretical strides in the field of quantum computing, the question of how to physically implement a qubit—still remains. Creating devices with high-performance features like extended coherence times, great controllability, etc. depends significantly on the material used for the qubit design. One of the prominent candidates for qubit architecture is superconducting qubits. The superconducting qubit modality has been utilized to demonstrate prototype algorithms in the noisy intermediate-scale quantum (NISQ) technology era, in which non-error-corrected qubits are used to implement quantum simulations and quantum algorithms [10]. Recently, Google announced the development of a quantum processor based on superconducting qubits that can complete specific tasks significantly faster than any supercomputer now in use [11]. A striking feature of superconducting qubits is that their energy-level spectra are governed by circuit element parameters and thus are configurable; they can be engineered to exhibit "atomlike" energy spectra with the desired properties. For this reason, superconducting qubits are also often referred to as

"artificial atoms," offering a rich parameter space of possible qubit properties and operation regimes, with predictable performance in terms of transition frequencies, anharmonicity, and complexity [12]. "The superconducting artificial atoms" are electronic circuits comprising lithographically defined Josephson tunnel junctions, inductors (L), capacitors (C), and interconnects [13].

Superconducting qubits store data in the quantum degrees of freedom of anharmonic oscillators that are nanofabricated from superconducting circuit components. They start off conceptually as simple harmonic oscillators known as linear LC resonant circuits, which are subsequently made to variable degrees anharmonic by the addition of a nonlinear inductive component known as the Josephson junction. These superconducting circuits behave as quantum mechanical oscillators (e.g., "artificial atoms") when cooled to dilution refrigerator temperatures (20 milliKelvin), exhibiting quantized states of electronic charge, magnetic flux, or junction phase depending on the design parameters of the individual circuit elements [13].

There are three main superconducting qubit archetypes: charge qubits, flux qubits and phase qubits [14]. We can distinguish between these three types of superconducting qubits according to the ratio E_J/E_C, where E_J is Josephson energy and E_C is charging energy.

2.10 The Transmon Qubit

One of the most important platforms for quantum research and computation is a superconducting transmon qubit. The first controlled qubit-qubit interaction with fidelities greater than 0.99 in multi-qubit systems was demonstrated with the transmon qubit [10] in 2014. Since then, numerous controlled two-qubit interactions have been shown to have similarly high fidelities. A transmon is a particular kind of superconducting charge qubit that was created with the intention of having less sensitivity to charge noise. It is used in quantum computing, and more especially in superconducting quantum computing. At Yale University, Robert J. Schoelkopf, Michel Devoret, Steven M. Girvin, and others created the transmon in [15, 16]. Its name is an acronym for the phrase "transmission line shunted plasma oscilla-

tion qubit," which refers to a type of qubit that uses capacitively shunted superconductors in a Cooper-pair box to reduce the susceptibility to charge noise while preserving enough anharmonicity for selective qubit control [17].

By substantially increasing the Josephson energy to charging energy ratio, the transmon achieves its reduced sensitivity to charge noise. This is achieved by using a sizable shunting capacitor. Offset charge-independent energy level spacings are formed as a result. For planar on-chip transmon qubits, T_i coherence times (periods) range between 30 to 40 μs [18]. By using a three-dimensional superconducting cavity instead of a superconducting transmission line cavity, recent work on transmon qubits has considerably improved T_i times to 95 s. These findings show that Josephson junction losses did not constrain earlier T_i times. Research is being done to better understand the fundamental constraints on the coherence time in superconducting qubits like the transmon [19].

A superconducting transmon qubit, which is formed of superconducting materials like niobium and aluminum and printed on a silicon substrate, is the physical type of qubit used by the quantum computers you interact with in IBM Quantum. Such systems are not naturally occurring qubits; rather, the qubit is created by selecting two energy levels from a large number of states [20].

Qubit relaxation and coherence times will need to be significantly increased in order to allow for the construction of large, practical quantum systems based on transmon qubits. These times are currently constrained by the bulk characteristics of the component materials. This shows that uncontrolled surfaces, interfaces, and contaminants are probably where relaxation or decoherence starts. For the transmon qubit, any arbitratry single qubit rotation axis can be chosen in the xy plane by tuning the phase of the microwave drive

The Hamiltonian of the transmon qubit can be concisely written in the form

$$H = 4E_c n^2 - E_j \cos(\phi)$$

Here, $E_c = e^2/\left(2C_\Sigma\right), C_\Sigma = C_s + C_j$ represents the total capacitance comprising of the shunt capacitance, C_s and the self-capacitance of the junction C_j.

$E_j = I_c\phi_0/2\pi$ is the Josephcon energy and I_c is the critical current of the junction [10]

Over the past years, the superconducting quit community has converged toward circuit designs where $E_j \gg E_c$. This is because when $E_j \leq E_c$, the quit becomes more susceptible to charge noise making it extremely difficult to obtain high coherence.

Chapter 3

Two-Step Single Qubit Gate Operations With Rotations Axes Fixed in A Single Plane

3.1 Two-Step Single Qubit Gate Operations With Rotations Axes Fixed in the XZ Plane

In this section, we present a brief overview of a previous work that has been done in this research area. Our key material is [21]. In [21], the authors studied single-qubit gates [22] that involve two fixed steps with rotation axes in a single plane. They showed that if the rotation axes are tuned in an arbitrary direction in a fixed plane, then only two rotation steps and one rotation step are sufficient for the implementation of a single-qubit gate and for the implementation of a state transformation, respectively.

In Sec. III of [21], the authors presented a detailed proof of single-qubit gates via two-step qubit rotations, wherein they considered the rotation axes that point in an arbitrary direction in a single plane. For this purpose, they required the solution of the rotation parameters to be defined by

$$R(\hat{n}, \phi) = e^{i\eta} R_2(\hat{n}_2, \phi_2) R_1(\hat{n}_1, \phi_1), \tag{3.1}$$

where $\hat{n}$ shows the rotation axis which can point anywhere in the Bloch sphere [23], however, the individual rotation axes, such as, $\hat{n}_2$ and $\hat{n}_1$ lie in the xz plane only. Since we

are dealing with rotations, the authors found it more convenient to transform to angular coordinates which are specified by

$$\hat{n} = (\sin\theta\cos\psi, \sin\theta\sin\psi, \cos\theta), \tag{3.2}$$

$$\hat{n}_1 = (\sin\theta_1, 0, \cos\theta_1), \tag{3.3}$$

$$\hat{n}_2 = (\sin\theta_2, 0, \cos\theta_2). \tag{3.4}$$

Many solutions do exist for the equation (3.1) above and the authors worked out one of such solutions. The problem was first simplified by transforming to a new set of coordinate axes defined by the projection of the logical rotation axis $\hat{n}$ onto the xz plane, where the normalized projection becomes the new $\hat{z}$ axis, as shown in Fig. 2(b) of the main text of the paper. The new coordinate system was described by primed variables which were achieved by rotating the original coordinate axes around $\hat{y}$ axis. After the rotation, the $\hat{y}$ axis remained unchanged, while the $\hat{x}$ and $\hat{z}$ axes became $\hat{x}'$ and $\hat{z}'$.

$$\hat{n} = \sin\theta'\hat{y}, \cos\theta'\hat{z}, \tag{3.5}$$

where

$$\sin\theta' = \sin\theta\sin\psi. \tag{3.6}$$

The detailed solution of the newly defined coordinate system is provided in Appendix B of the subject paper [24].

Further, Pauli operators were used to obtain various relations in the primed coordinate system and from numerical analysis, it was found that there will be a continuum of solutions for the resultant equations. However, upon imposing some constraints on the parameters, the set of equations were simplified to only three equations with two unknown parameters, i.e., ϕ_1 and θ_1'. After a straightforward algebra, the following two equations obtained were:

$$k\cos\theta'\sin\frac{\phi}{2} = \cos\frac{\phi_1'}{2}. \tag{3.7}$$

$$k\sin\theta'\tan\frac{\phi}{2} = -\tan\frac{\theta_1'}{2}. \tag{3.8}$$

From these two equations, it was uniquely determined that ϕ_1 lies in the range $[0, 2\pi]$ and θ_1' lies in the range $[0, \pi]$. It is worthy of note that, this was not the only solution as ϕ_2 and θ_2' can also be uniquely determined by imposing some different constraints. The conventional Euler method could be used to implement any desired single-qubit gate in three rotation steps (e.g.$X = e^{in} R_z(\alpha) R_y(\beta) R_z(\gamma)$, for some specific α, β, γ). In the paper [21], the authors provided a constructive proof that any single-qubit gate (up to a global phase) can be generated in two rotation steps, when the rotation axes point in an arbitrary direction in a single plane. The authors also proposed that their findings may be useful in different logical qubits, especially in the decoherence free subspaces and subsystems of three-spin logical qubits, such as exchange-only qubits. The authors also proposed that their findings could be applied to any qubit implementation which has at least partial control over the rotation axes [25, 26, 27].

3.2 Two-Step Single Qubit Gate Operations With Rotations Axes Fixed in The XY Plane

Our work was concerned with demonstrating that, any single qubit gate operation could be implemented in two sequential steps when the two rotation axes are fixed in a specific plane (in our work, we used the xy-plane).

An arbitrary single-qubit rotation can be implemented with at most three rotations around fixed orthogonal axes

$$R(\hat{n}, \phi) = e^{in} R(\hat{n}_2, \phi_2) R(\hat{n}_1, \phi_1) \tag{3.9}$$

Here, we implement single-qubit gates with two sequential rotations by fixing the rotation axes in the xy plane. For a standard superconducting qubit (transmon qubit), the single qubit rotation axis can be chosen in the xy-plane by tuning the phase of the microwave drive.

We provide a constructive proof that for rotation axes pointing arbitrarily in a single

plane, any single qubit gate (up to a global phase) can be implemented in two steps. We want to specifically solve for the rotation parameters defined by

$$R(\widehat{\mathbf{n}}, \phi) = e^{i\eta} R(\widehat{\mathbf{n}}_2, \phi_2) R(\widehat{\mathbf{n}}_1, \phi_1) \tag{3.10}$$

Here, the rotation axis $\widehat{\mathbf{n}}$ can point anywhere in the Bloch sphere, but the individual rotation axes $\widehat{\mathbf{n}}_1$ and $\widehat{\mathbf{n}}_2$ are constrained to lie in the xy plane. It is convenient to work with angular coordinates established by:

$$\hat{n} = (\sin\theta\cos\psi, \sin\theta\sin\psi, \cos\theta)$$

$$\hat{n_1} = (\sin\theta_1, 0, \cos\theta_1)$$

$$\hat{n_2} = (sin\theta_2, 0, cos\theta_2).$$

The right-hand side of equation (3.10) has five parameters $(\eta, \theta_1, \phi_1, \theta_2, \phi_2)$ while the left hand side (an arbitrary qubit rotation) has three parameters (θ, ψ, ϕ). As a result, the equation is clearly under-constrained; many solutions exist, any of which suits our needs.

We now provide an explicit, analytical formulation to show that there is at least one solution to the above equation (Eq. 3.10). By transforming the problem to a new set of coordinate axes determined by the projection of the rotation axis $\hat{n}$ onto the xy-plane, we first make the problem simpler and the normalised projection serves as our new x-axis as shown in figure 3.2.1 below. We observe that $\widehat{\mathbf{z}}$ is the same in both coordinate systems.

Projecting $\widehat{\mathbf{n}}$ onto the xy-plane, in the new coordinate system (x', y', z)

$$\widehat{\mathbf{n}} = (\sin\theta, 0, \cos\theta)$$
$$\widehat{\mathbf{n}}_1 = (\cos\psi_1', \sin\psi_1', 0)$$
$$\widehat{\mathbf{n}}_2 = (\cos\psi_2', \sin\psi_2', 0) \quad \psi_i' = \psi_i - \psi$$

Our goal is to identify two successive rotation steps around axes in the xy plane that produce an arbitrary single-qubit gate, up to a global phase.

$$R(\widehat{\mathbf{n}}, \phi) = e^{i\eta} R(\widehat{\mathbf{n}}_2, \phi_2) R(\widehat{\mathbf{n}}_1, \phi_1) \tag{3.11}$$

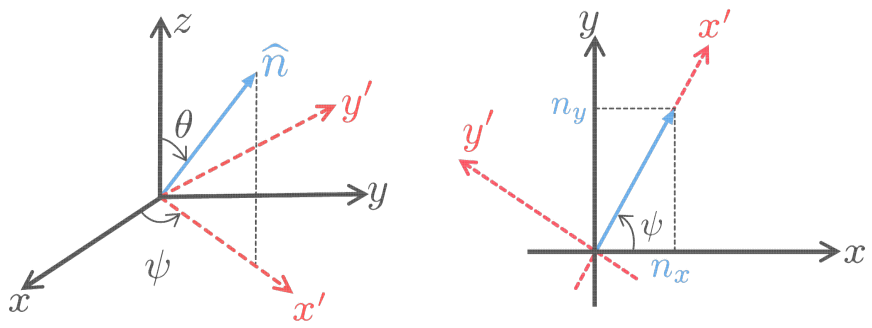

Figure 3.2.1: (a) The rotation axis $\hat{n}$ with the polar angle θ and the azimuthal angle ψ. (b) The projection of $\hat{n}$ onto the xy-plane. A new coordinate system is established with axes $\hat{x}'$ and $\hat{y}'$, such that $n'_y = 0$, by rotating the xy plane around the y axis by angle θ

The rotation operator can be expressed in terms of Pauli operators as follows:

$$\begin{aligned}\mathcal{R}(\hat{n},\phi) &= \exp\left[-i\frac{\sigma\cdot\hat{n}}{2}\phi\right] \\ &= I\cos\frac{\phi}{2} - i\sigma\cdot\hat{n}\sin\frac{\phi}{2}\end{aligned}$$

But $\hat{n} = (\sin\theta, 0, \cos\theta) = \sin\theta\hat{x} + \cos\theta\hat{z}$, so

$$R(\hat{n},\phi) = I_{2\times2}\cos\frac{\phi}{2} - i\sin\frac{\phi}{2}[(\sigma_x\hat{x}+\sigma_y\hat{y}+\sigma_z\hat{z})(\sin\theta\hat{x}+\cos\theta\hat{z})] \tag{3.12}$$

So we find

$$\begin{aligned}&(\sigma_x\hat{x}+\sigma_y\hat{y}+\sigma_z\hat{z})(\sin\theta\hat{x}+\cos\theta\hat{z}) \\ &= \sigma_x\hat{x}(\sin\theta\hat{x}+\cos\theta\hat{z}) + \sigma_y\hat{y}(\sin\theta\hat{x}+\cos\theta\hat{z}) + \sigma_z\hat{z}(\sin\theta\hat{x}+\cos\theta\hat{z}) \\ &= (\sin\theta\sigma_x + \cos\theta\sigma_z).\end{aligned} \tag{3.13}$$

$$R(\hat{n},\phi) = I_{2\times2}\cos\frac{\phi}{2} - i\sin\frac{\phi}{2}\left[\sin\theta\sigma_x + \cos\theta\sigma_z\right]$$

On the RHS, we first consider $R(\hat{n}_1,\phi_1)$

$$R(\hat{n}_1,\phi_1) = I_{2\times2}\cos\frac{\phi_1}{2} - i\sin\frac{\phi_1}{2}\sigma\hat{n}_1$$

But

$$\hat{n}_1 = (\cos\psi_1', \sin\psi_1^1, 0) = \cos\psi_1'\hat{x} + \sin\psi_1'\hat{y} + 0$$

So

$$R(\hat{n}_1, \phi_1) = I_{2\times 2}\cos\frac{\phi_1}{2} - i\sin\frac{\phi_1}{2}\left[(\sigma_x\hat{x} + \sigma_y\hat{y} + \sigma_z\hat{z})(\cos\psi_1'\hat{x} + \sin\psi_1'\hat{y})\right]$$

Now, we find

$$(\sigma_x\hat{x} + \sigma_y\hat{y} + \sigma_z\hat{z})(\cos\psi_1'\hat{x} - \sin\psi_1'\hat{y}) = \cos\psi_1'\sigma_x + \sin\psi_1'\sigma_y \tag{3.14}$$

$$\begin{aligned} R(\hat{n}_1, \phi_1) &= I_{2\times 2}\cos\frac{\phi_1}{2} - i\sin\frac{\phi_1}{2}\left[\cos\psi_1'\sigma_x + \sin\psi_1'\sigma_y\right] \\ &= I_{2\times 2}\cos\frac{\phi_1}{2} - i\ \sin\frac{\phi_1}{2}\cos\psi_1'\sigma_x - i\ \sin\frac{\phi_1}{2}\sin\psi_1'\sigma_y \end{aligned}$$

Next, we consider $R(\hat{n}_2, \phi_2)$:

$$R(\hat{n}_2, \phi_2) = I\cos\frac{\phi_2}{2} - i\sin\frac{\phi_2}{2}[\hat{\sigma}\cdot\hat{n_2}] \tag{3.15}$$

but

$$n_2 = (\cos\psi_2\hat{x}, \sin\psi_2, 0) = \cos\psi_2'\hat{x} + \sin\psi_2\sigma_y$$

So

$$R(\hat{\eta}_2, \phi_2) = I\cos\frac{\phi_2}{2} - i\sin\frac{\phi_2}{2}\left[\left(\sigma_x\hat{x} + \sigma_y'\hat{y} + \sigma_z\hat{y}\right)(\cos\psi_2'\hat{z} + \sin\psi_2'\hat{y})\right]$$

Therefore

$$R(\hat{n}_2, \phi_2) = I_{2\times 2}\cos\frac{\phi_2}{2} - i\sin\frac{\phi_2}{2}\cos\psi_2'\sigma_x - i\sin\frac{\phi_2}{2}\sin\psi_2'\sigma_y.$$

We recall that

$$R(\hat{n}, \phi) = e^{in}R(\hat{n}_2, \phi_2)\,R(\hat{n}_1, \phi_2)\,.$$

Now the RHS is given by

$$\text{RHS} = e^{in}R(\hat{n}_2, \phi_2)\,R(\hat{n}_1, \phi_1)$$

$$\text{RHS} =$$

$$\mathrm{e}^{in}\left(I\cos\tfrac{\phi_2}{2}-i\sin\tfrac{\phi_2}{2}\cos\psi_2'\sigma_x-i\sin\tfrac{\phi_2}{2}\sin\psi_2'\sigma_y\right)\cdot\left(I\cos\tfrac{\phi_1}{2}-i\sin\tfrac{\phi_1}{2}\cos\psi_1'\sigma_x-i\sin\tfrac{\phi_1}{2}\sin\psi_1'\sigma_y\right).$$

By expansion of the RHS, we obtain

$$\begin{aligned}\text{RHS}=e^{in}\Bigg[&\cos\frac{\phi_2}{2}\cos\frac{\phi_1}{2}-i\sin\frac{\phi_1}{2}\cos\frac{\phi_2}{2}\cos\psi_1'\sigma_x-i\sin\frac{\phi_1}{2}\cos\frac{\dot{\phi}_2}{2}\sin\psi_1'\sigma_y-\\ &i\sin\frac{\phi_2}{2}\cos\psi_2'\cos\frac{\phi_1}{2}\sigma_x-\sin\frac{\phi_2}{2}\cos\psi_2'\sin\frac{\phi_1}{2}\cos\psi_1'-i\sin\frac{\phi_2}{2}\cos\psi_2'\sin\frac{\phi_1}{2}\sin\psi_1'\sigma_z\\ &-i\cos\frac{\phi_1}{2}\sin\frac{\phi_2}{2}\sin\psi_2'\sigma_y+i\sin\frac{\phi_2}{2}\sin\psi_2'\sin\frac{\phi_1}{2}\cos\psi_1'\sigma_z-\sin\frac{\phi_2}{2}\sin\psi_2'\sin\frac{\phi_1}{2}\sin\psi_1'\Bigg].\end{aligned}$$

Grouping like Pauli matrices, we obtain

$$\begin{aligned}\text{RHS }=e^{in}\Bigg[&\cos\frac{\phi_2}{2}\cos\frac{\phi_1}{2}-\sin\frac{\phi_2}{2}\cos\psi_2'\sin\frac{\phi_1}{2}\cos\psi_1'-\sin\frac{\phi_2}{2}\sin\psi_2'\sin\frac{\phi_1}{2}\sin\psi_1'\\ &-\left(i\sin\frac{\phi_2}{2}\cos\psi_2'\cos\frac{\phi_1}{2}+i\sin\frac{\phi_1}{2}\cos\frac{\phi_2}{2}\cos\psi_1'\right)\sigma_x\\ &-\left(i\sin\frac{\phi_1}{2}\cos\frac{\phi_2}{2}\sin\psi_1'+i\cos\frac{\phi_1}{2}\sin\frac{\phi_2}{2}\sin\psi_2'\right)\sigma_y\\ &-\left(i\sin\frac{\phi_2}{2}\cos\psi_2'\sin\frac{\phi_1}{2}\sin\psi_1'-i\sin\frac{\phi_2}{2}\sin\psi_2'\sin\frac{\phi_1}{2}\cos\psi_1'\right)\sigma_z.\end{aligned}$$

We Recall again that

$$R(\hat{\eta},\phi)=e^{in}R\left(\hat{n}_2,\phi_2\right)R\left(\hat{n}_1,\phi_2\right).$$

Equating coefficients of the Pauli operators, we obtain:

$$\cos\frac{\phi}{2}=e^{in}\left[\cos\frac{\phi_2}{2}\cos\frac{\phi_1}{2}-\sin\frac{\phi_2}{2}\cos\psi_2'\sin\frac{\dot{\phi}_1}{2}\cos\psi_1'-\sin\frac{\phi_2}{2}\sin\psi_2'\sin\frac{\phi_1}{2}\sin\psi_1'\right] \tag{3.16}$$

$$\sin\theta\sin\frac{\phi}{2}=e^{in}\left[\sin\frac{\phi_2}{2}\cos\psi_2'\cos\frac{\phi_1}{2}+\sin\frac{\phi_1}{2}\cos\frac{\phi_2}{2}\cos\psi_1'\right] \tag{3.17}$$

$$\sin\frac{\phi}{2}\cos\theta=e^{in}\left[\sin\frac{\phi_2}{2}\cos\psi_2'\sin\frac{\phi_1}{2}\sin\psi_1'-\sin\frac{\phi_2}{2}\sin\psi_2'\sin\frac{\phi_1}{2}\cos\psi_1'\right] \tag{3.18}$$

$$0=\sin\frac{\phi_1}{2}\cos\frac{\phi_2}{2}\sin\psi_1'+\cos\frac{\phi_1}{2}\sin\frac{\phi_2}{2}\sin\psi_2'. \tag{3.19}$$

Numerical analysis suggest that there will be a continuum of solutions for these equations. In the next section, we demonstrate one of the solutions by setting $\phi_2=\pi$ and $\psi_2'=0$ This simplifies the equations and enables us to find an analytical solution.

3.3 Finding Analytical Solutions To The Single-Qubit Gate operations With Rotation Axes In The XY Plane

As mentioned earlier, we constructively obtain an explicit solution by fixing $\phi_2 = \pi$ and $\psi_2' = 0$.

$$\phi_2 = \pi, \quad \psi_2' = 0 \Longleftrightarrow R\left(\hat{n}_2, \phi_2\right) = R\left(\hat{x}', \pi\right) \tag{3.20}$$

Now, Eq. (3.17) becomes

$$\sin\theta \sin\frac{\phi}{2} = e^{in}\left[\sin\frac{\phi_2}{2}\cos\psi_2'\cos\frac{\phi_1}{2} + \sin\frac{\phi_1}{2}\cos\frac{\phi_2}{2}\cos\psi_1'\right]$$

$$= e^{in}\left[\sin\frac{\pi}{2}\cos 0\cos\frac{\phi_1}{2} + \sin\frac{\phi_1}{2}\cos\frac{\pi}{2}\cos\psi_1'\right]$$

$$= e^{in}\left[\sin 90(1)\cos\frac{\phi_1}{2} + 0\right]$$

So

$$\sin\theta \sin\frac{\phi}{2} = e^{in}\cos\frac{\phi_1}{2}. \tag{3.21}$$

Eq. (3.18) becomes

$$\sin\frac{\phi}{2}\cos\theta = e^{in}\left[\sin\frac{\phi_2}{2}\cos\psi_2'\sin\frac{\phi_1}{2}\sin\psi_1' - \sin\frac{\phi_2}{2}\sin\psi_2'\sin\frac{\phi_1}{2}\cos\psi_1'\right]$$

$$= e^{in}\left[\sin\frac{\pi}{2}\cos 0\sin\frac{\phi_1}{2}\sin\psi_1' - \sin\frac{\pi}{2}\sin 0\sin\frac{\phi_1}{2}\cos\psi_1'\right]$$

$$= e^{in}\left[\sin 90\cos 0\sin\frac{\phi_1}{2}\sin\psi_1^1\right]$$

So

$$\sin\frac{\phi}{2}\cos\theta = e^{in}\sin\frac{\phi_1}{2}\sin\psi_1'. \tag{3.22}$$

Finally, Eq. (3.16) becomes:

$$\cos\frac{\phi}{2} = e^{in}\left[\cos\frac{\phi_2}{2}\cos\frac{\phi_1}{2} - \sin\frac{\phi_2}{2}\cos\psi_2'\sin\frac{\phi_1}{2}\cos\psi_1' - \sin\frac{\phi_2}{2}\sin\psi_2'\sin\frac{\phi_1}{2}\sin\psi_1'\right]$$

$$= e^{in}\left[\cos\frac{\pi}{2}\cos\frac{\phi_1}{2} - \sin\frac{\pi}{2}\cos 0\sin\frac{\phi_1}{2}\cos\psi_1' - \sin\frac{\pi}{2}\sin 0\sin\frac{\phi_1}{2}\sin\psi_1'\right]$$

$$= e^{in}\left[\cos\frac{90}{2}\cos\frac{\phi_1}{2} - \sin 90\cos 0\sin\frac{\phi_1}{2}\cos\psi_1^1 - \sin 90\sin 0\sin\frac{\phi_1}{2}\sin\psi_1'\right]$$

$$= e^{in}\left[-\sin\ 90\cos 0\sin\frac{\phi_1}{2}\cos\psi_1' - 0\right]$$

So

$$\cos\frac{\phi}{2} = -e^{in}\sin\frac{\phi_1}{2}\cos\psi_1'. \tag{3.23}$$

Using Eqs. (3.21) and (3.22), we get

$$\cos\theta\tan\frac{\phi}{2} = \frac{e^{in}\sin\psi_1'\sin\dfrac{\phi_1}{2}}{-e^{in}\cos\psi_1'\sin\dfrac{\phi_1}{2}} = -\frac{\sin\psi_1'}{\cos\psi_1'} = -\tan\psi_1'.$$

We now have two equations:

$$\sin\theta\sin\frac{\phi}{2} = e^{in}\cos\frac{\phi_1}{2},$$

$$\cos\theta\tan\frac{\phi}{2} = -\tan\psi_1'$$

From these equations, we can determine the unknown parameters ϕ_1 and ψ_1'. In effect, we are able to determine the parameters which are needed to implement a two-step qubit rotation

Below, we consider a few cases where this two-step qubit rotation was utilized.

Example 1. *Hadamard Gate:*

$$H = \frac{1}{\sqrt{2}}\begin{pmatrix} 1 & 1 \\ 1 & -1 \end{pmatrix} = iR(\widehat{\mathbf{n}},\pi), \quad \widehat{\mathbf{n}} = \left(\frac{1}{\sqrt{2}}, 0, \frac{1}{\sqrt{2}}\right)$$

$$H = iR(\widehat{\mathbf{x}},\pi)R\left(\widehat{\mathbf{y}},\frac{\pi}{2}\right).$$

As shown above, we observe that the Hadamard gate can be successfully implemented with only two-sequential rotations first around the y-axis by an angle $\pi/2$ and next around the x-axis by an angle π.

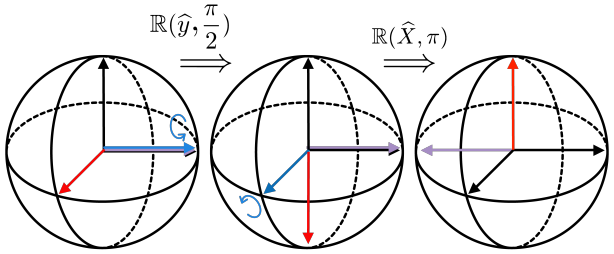

Figure 3.3.1: Implementation of Hadamard gate in two steps

Example 2. *Pauli Z Gate:*

$$R(\widehat{\mathbf{z}}, \phi) = -R\left(\widehat{\mathbf{n}}_2, \pi\right) R(\widehat{\mathbf{x}}, \pi) \quad \widehat{\mathbf{n}}_2 = \left(\cos\frac{\phi}{2}, \sin\frac{\phi}{2}, 0\right)$$

for $\phi = \pi/2$

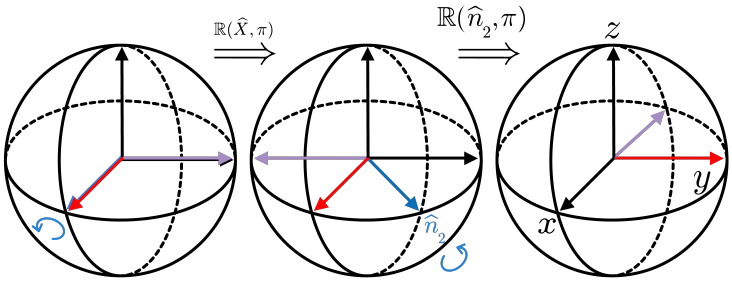

Figure 3.3.2: Implementation of Z gate in two steps

Here, we observe that the Z gate can be successfully implemented with only two-sequential rotations: first around the x-axis by an angle $\pi/2$ and next around the $\widehat{\mathbf{n}}_2$-axis

$$\widehat{\mathbf{n}}_2 = \left(\cos\frac{\phi}{2}, \sin\frac{\phi}{2}, 0\right)$$

by an angle π.

Chapter 4

Numerical Solutions for Two-Step Single Qubit Gates

4.1 Numerical Optimization

Optimization is the process of making something as good and efficient as possible. Mathematical optimization is the process of effectively locating the least value of a particular objective function by choosing input values from a domain set(a set which is subject to some constraints) and determining the function's value. In decision science and the analysis of physical systems, optimization is a crucial tool. To make use of this tool, we must first identify some objective, a quantitative gauge of the performance of the system under study. The objective could be time, profit, potential energy, or any quantity or group of quantities that can be represented by a single number. The objective is dependent on specific characteristics of the system, called variables. The goal is to determine specific values of the variables that optimize the objective. The variables are usually subject to some constraints and to ensure the acceptability of the solution, those constraints must be satisfied. Thus in optimization, the decision-maker or modeler typically seeks to find the 'absolutely best' decision which corresponds to the minimum (or maximum) of a suitable objective function, while it satisfies a given set of feasibility constraints [28]. For example, the electron density in a molecule or the interest rate on a loan are quantities that are constrained to be non-negative [29]. Using an optimization procedure and typically a computer, the solution to a model can be found once the model has been created. At present, there is no single optimization algorithm that can be used to solve all optimization problems; rather, there are a variety of algorithms,

each of which is designed to solve a specific kind of optimization problem. Choosing the best algorithm for a given application is the user's responsibility. The choice is vital because it could affect how quickly or how slowly the problem is solved—or even whether a solution is ever discovered. After an optimization algorithm has been applied to the model, we must be able to determine whether the algorithm has succeeded in its task of finding a solution. Oftentimes, there are elegant mathematical formulae known as optimality criteria for verifying whether the current set of variables is indeed the solution of the problem. If the optimality criteria are not satisfied, they may give useful information on how the current estimate of the solution can be improved. By using methods like sensitivity analysis, which indicates the sensitivity of the answer to changes in the model and data, the model may be improved [29]. The solution's application-specific interpretation may also suggest modifications or enhancements that could be made to the model (or corrected). Any modifications to the model result in a new optimization issue being solved, and the process is then repeated.

In our work, we sought to gain optimal two-step gate control (operation) by finding a set of control parameters that minimize the cost function (subject to some constraints). A cost function (performance measure) calculates how far a system's performance deviates from its ideal performance. Gate infidelity is a logical choice for the cost function in unitary gate optimization.

In our work, we defined the cost function by:

$$A = Norm\left[M_T - R_m(t)\right]$$

where M_T and $R_m(t)$ are the target and the final unitary gates, respectively, and the norm of the matrix, is the square root of the sum of the squares of all its elements. For the ideal gate operation, $A = 0$.

There are two types of optimization algorithms: gradient-based and gradient-free. To successfully define an optimal solution by any gradient-based algorithm, the extreme (optimal) point is obtained when the gradient's value zero [30]. In gradient-based algorithms, for instance, the performance of a particular pulse may be evaluated by the cost function. And,

the control parameters are updated for the next iteration based on the derivative of the cost function with respect to the control parameters. The advantage of gradient-based algorithms is that they are much faster than gradient-free algorithms. However, gradient-based algorithms do not work well if the cost function is discontinuous or noisy because calculating the gradient is difficult in such a case. Thus, they are difficult to use for direct optimization on an experimental system, i.e., closed-loop optimal control.

Despite their slowness, gradient-free algorithms are simple to implement and work well with a noisy measurement outcome, suggesting that we can perform closed-loop optimal control using these algorithms. Thus, gradient-free algorithms are useful for the calibration or optimization of pulses defined by a limited number of parameters.

There are many numerical optimization algorithms that have been used widely in quantum control. In this work, we used BlackBoxOptim.jl [31] because it has been found to be one of the most reliable algorithms for optimizing quantum gate parameters. BlackBoxOptim.jl is a gradient-free optimization algorithm.

4.1.1 Global Optimization

In applied science and mathematical analysis, finding the global minima or maxima of a given function or group of functions on a given set is known as global optimization. Global optimization is concerned with computing and describing global solutions to nonconvex continuous, mixed-integer, differential-algebraic, bilevel, and non-factorable problems. Global optimization is utilized for problems with a small number of variables, where computing time is not critical, but the value of finding the true global solution is very high [32] .

Given an objective function g that is to be minimized and a set of equality and inequality constraints, the basic goal of global optimization is to find an epsilon global minimum of the objective function g subject to the set of constraints T [33].

Furthermore, global optimization concentrates on the critical problems of how to establish lower and upper bounds on the global minimum of the objective function g that are valid for the entire feasible region T, as well as how to identify a group of high-quality local solutions

close to the global solution. Multi-modal optimization in global optimization occurs when a function has multiple global optimum points, each of which has a unique input and the same objective function evaluation. There is always a global optima for an objective function, and there may also be a local optima, which typically has an assessment of an objective function but is less desirable than the global optima. Since the goal of global optimization is to find the global optima, it is also known as a global search algorithm. The main goal is to precisely locate the function's extrema by navigating the whole input search space. Global optimization is also called minimization problem, and the reason is that the maximization of real valued function $g(x)$ is similar to the minimization of the function

$f(x) := (-1).g(x)$

Examples of global search algorithm include:

- Particle swarm optimization
- Genetic Algorithm
- Simulated Annealing [34].

4.2 Numerical Code

The rotation axis $\hat{n}$ is described by the angle λ as shown below:

Given a rotation axis $\hat{n}$ that is fixed in the xy plane, an arbitrary rotation around $\hat{n}$ by an angle ϕ is given by

$$\widehat{R}_n(\phi) = \exp\left[-i\frac{\phi}{2}\hat{n}\cdot\vec{\sigma}\right] = \cos\frac{\phi}{2}I_{2\times 2} - i\sin\frac{\phi}{2}\hat{n}\cdot\vec{\sigma},$$

where $\vec{\sigma} = \sigma_x\hat{x} + \sigma_y\hat{y} + \sigma_z\hat{z}$ and $\hat{n} = \cos\lambda\hat{x} + \sin\lambda\hat{y}$

Therefore,

$$\widehat{R}_n(\phi) = \cos\frac{\phi}{2}I_{2\times 2} - i\sin\frac{\phi}{2}\left[(\cos\lambda\hat{x} + \sin\lambda\hat{y})\,(\sigma_x\hat{x} + \sigma_y\hat{y} + \sigma_z\hat{z})\right] \tag{4.1}$$

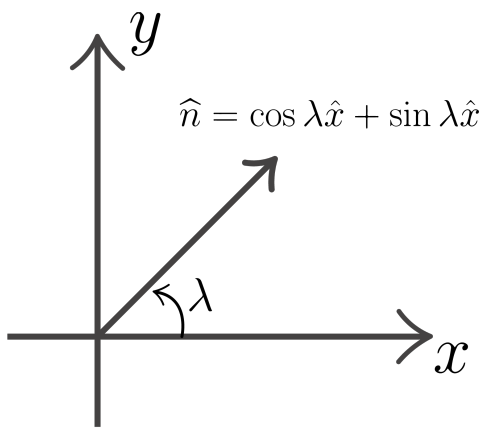

Figure 4.2.1: Rotation axis $\hat{n}$

We find that,

$$(\cos\lambda\hat{x} + \sin\lambda\hat{y})\,(\sigma_x\hat{x} + \sigma_y\hat{y} + \sigma_z\hat{z})$$

$$= \cos\lambda\sigma_x\hat{x}\cdot\hat{x} + \cos\lambda\sigma_y\hat{y}\cdot\hat{x} + \cos\lambda\sigma_z\hat{z}\cdot\hat{x} + \sin\lambda\sigma_x\hat{x}\cdot\hat{y} + \sin\lambda\sigma_y\hat{y}\cdot\hat{y} + \sin\lambda\sigma_z\hat{z}\cdot\hat{y}$$

$$= \cos\lambda\sigma_x + \sin\lambda\sigma_y.$$

So,

$$\begin{aligned}
\widehat{R}_{n(\lambda)}(\phi) &= \cos\frac{\phi}{2}I_{2\times 2} - i\sin\frac{\phi}{2}\left(\cos\lambda\sigma_x + \sin\lambda\sigma_y\right) \\
&= \begin{pmatrix} \cos\frac{\phi}{2} & 0 \\ 0 & \cos\frac{\phi}{2} \end{pmatrix} - i\sin\frac{\phi}{2}\left[\begin{pmatrix} 0 & \cos\lambda \\ \cos\lambda & 0 \end{pmatrix} + \begin{pmatrix} 0 & -i\sin\lambda \\ i\sin\lambda & 0 \end{pmatrix}\right] \\
&= \begin{pmatrix} \cos\frac{\phi}{2} & 0 \\ 0 & \cos\frac{\phi}{2} \end{pmatrix} - \begin{pmatrix} 0 & i\sin\frac{\phi}{2}(\cos\lambda - i\sin\lambda) \\ i\sin\frac{\phi}{2}(\cos\lambda + i\sin\lambda) & 0 \end{pmatrix}
\end{aligned}$$

Therefore,

$$\widehat{R}_{n(\lambda)}(\phi) = \begin{pmatrix} \cos\frac{\phi}{2} & -i\sin\frac{\phi}{2}(\cos\lambda - i\sin\lambda) \\ -i\sin\frac{\phi}{2}(\cos\lambda + i\sin\lambda) & \cos\frac{\phi}{2} \end{pmatrix} \tag{4.2}$$

Accordingly, the two rotations around two axes that have been fixed in the xy-plane are given

by:

$$\widehat{R}_{n_1(\lambda_1)}(\phi_1) = \begin{pmatrix} \cos\frac{\phi_1}{2} & -i\sin\frac{\phi_1}{2}\left(\cos\lambda_1 - i\sin\lambda_1\right) \\ -i\sin\frac{\phi_1}{2}\left(\cos\lambda_1 + i\sin\lambda_1\right) & \cos\frac{\phi_1}{2} \end{pmatrix} \tag{4.3}$$

And

$$\widehat{R}_{n_2(\lambda_2)}(\phi_2) = \begin{pmatrix} \cos\frac{\phi_2}{2} & -i\sin\frac{\phi_2}{2}\left(\cos\lambda_2 - i\sin\lambda_2\right) \\ -i\sin\frac{\phi_2}{2}\left(\cos\lambda_2 + i\sin\lambda_2\right) & \cos\frac{\phi_2}{2} \end{pmatrix} \tag{4.4}$$

We proceed to write a code that decomposes any single-qubit gate into $e^{i\theta}R_{\hat{n}_2(\lambda_2)}(\phi_2)\,R_{\hat{n}_1(\lambda_1)}(\phi_1)$. In this case, $e^{i\theta}$ is the global phase of the single-qubit.

We do this by first writing a function $R_m(t)$ that takes input values ($t[1]$, $t[2]$, $t[3]$, $t[4]$, $t[5]$) and returns a product matrix $\widehat{R}_{n_1(\lambda_1)}(\phi_1)\widehat{R}_{n_2(\lambda_2)}(\phi_2$.

Here,

$$\theta = t[1], \quad \phi_1 = t[2], \quad \phi_2 = t[3], \quad \lambda_1 = t[4], \quad \lambda_2 = t[5].$$

Next, we write a function that computes A.

$$A = Norm\left[M_T - R_m(t)\right]$$

Next, we call the BlackBoxOptim.jl optimization package to output the optimal parameters θ, ϕ_1, ϕ_2, λ_1, and λ_2.

The BlackBoxOptim.jl is a global optimization package for Julia Programming Language that supports multi-objective and single-objective optimization problems. It is focused on heuristic, metaheuristic, and stochastic algorithms that do not require the function being optimized to be differentiable. This contrasts with older, more conventional deterministic algorithms, which are dependent on gradients or differentiability. This is in contrast to more traditional, deterministic algorithms that are often based on gradients or differentiability. BlackBoxOptim.jl also supports parallel evaluation to speed up optimization for functions with sluggish evaluation times [31]. The code was run for several single qubit gates, and the output results were put into the cost function A to determine the fitness of the outputs.

4.3 Numerical results

In this section, we present the ouputs of our code by listing the output parameters and verifying the fitness of the parameters. In BlackBoxOptim.jl package, the fitness of a cost function determines how close the function is to the desired (target) results. Conventionally, a fitness of 0.000 represents highly efficient output parameters.

4.3.1 Numerical Solution for the Hadamard Gate

The Hadamard gate is given by the following matrix:

$$H = \frac{1}{\sqrt{2}} \begin{pmatrix} 1 & 1 \\ 1 & -1 \end{pmatrix}$$

When the BlackBoxOptim.jl package was run, the output results of the Hadamard gate were as follows:

Best values found:

$$(-1.5708, -3.01731, 1.57851, 6.22092, -1.69484)$$

Thus,

$$\theta = -1.5708, \phi_1 = -3.01731, \phi_2 = 1.57851, \lambda_1 = 6.22092, \lambda_2 = -1.69484.$$

These 5 output values were put back into the initial function to verify their fitness. The resulting matrix obtained was:

$$R_m = \begin{pmatrix} 0.707107 - 5.6 \cdot 10^{-6} i & 0.707106 - 5.9 \cdot 10^{-8} i \\ 0.707106 - 5.1 \cdot 10^{-6} i & -0.707107 - 4.1 \cdot 10^{-7} i \end{pmatrix}$$

Fitness: 0.000000000

This 2 by 2 matrix output exactly corresponds to the Hadamard gate. The fitness is 0.000000 implying a very efficient output.

4.4 Numerical Solution for the Phase Gate

The Phase gate has the matrix representation,

$$P = \begin{pmatrix} 1 & 0 \\ 0 & e^{i\phi} \end{pmatrix}$$

When the BlackBoxOptim.jl package was run the output results for the Phase gate were as follows:

Best candidate found:

$$(-3.14159, 2.446 \cdot 10^{-16}, -6.28319, -0.812379, 2.27736).$$

Here,

$$\theta = -3.14159, \phi_1 = 2.446 \cdot 10^{-16}, \phi_2 = -6.28319, \lambda_1 = -0.812379, \lambda_2 = 2.27736.$$

To verify these 5 output values, they were reinserted into the initial function. The resulting matrix was as follows:

$$R_m = \begin{pmatrix} 1.0 + 2.7 \cdot 10^{-6} i & 1.8 \cdot 10^{-6} - 1.5 \cdot 10^{-6} i \\ -1.8 \cdot 10^{-6} - 1.5 \cdot 10^{-6} i & 1.0 + 2.7 \cdot 10^{-6} i \end{pmatrix}.$$

Fitness: 0.000000000.

This 2 by 2 output matrix precisely matches the Phase gate. The fitness of 0.000000 indicates optimal output results.

4.5 Numerical Solution for the T Gate

The T Gate is given by

$$T = e^{i\pi/8} \begin{pmatrix} e^{-i\pi/8} & 0 \\ 0 & e^{i\pi/8} \end{pmatrix}$$

Upon running the BlackBoxOptim.jl package, the output results for the T gate were as follows:

Best candidate found:

$$(3.53429, 3.14159, -3.14159, 4.67466, 1.92577).$$

Here,

$$\theta = 3.53429, \phi_1 = 3.14159, \phi_2 = -3.14159, \lambda_1 = 4.67466, \lambda_2 = 1.92577.$$

These output values were also put into the initial function and the corresponding matrix obtained was:

$$R_m = \begin{pmatrix} 1.0 - 5.3 \cdot 10^{-6} i & -2.5 \cdot 10^{-6} - 6.0 \cdot 10^{-7} i \\ 2.2 \cdot 10^{-6} - 6 + 1.4 \cdot 10^{-6} i & 0.707105 + 0.7i \end{pmatrix}.$$

Fitness: 0.000000000.

This 2 by 2 output matrix precisely matches the T gate.

Similar success was achieved in optimizing the parameters of the remaining single qubit gates, including the S gate, S dagger gate, Pauli X gate, Pauli Y gate, the Pauli Z gate and the Identity gate. Below is a display of the outcomes:

4.6 Numerical Solution for the S Gate

Best candidate found:

$$(3.92699, -3.14159, 3.14159, -6.24679, 3.96339).$$

Here,

$$R_m = \begin{pmatrix} 1.0 - 4.7 \cdot 10^{-6} i & 8.6 \cdot 10^{-7} - 2.3 \cdot 10^{-6} i \\ 2.3 \cdot 10^{-6} - 8.6 \cdot 10^{-7} i & -3.1 \cdot 10^{-6} e + 1.0 i \end{pmatrix}$$

Fitness: 0.000000000.

4.7 Numerical Solution for the $S^\dagger$ Gate

Best candidate found:

$$(-3.92699, 3.14159, -3.14159, 6.17526, -4.03491).$$

Here,

$$R_m = \begin{pmatrix} 1.0 - 5.3 \cdot 10^{-6} - 6i & 6.9 \cdot 10^{-7} + 2.4 \cdot 10^{-6} i \\ 2.4 \cdot 10^{-6} + 6.9 \cdot 10^{-7} i & 6.9 \cdot 10^{-6} - 1.0i \end{pmatrix}.$$

Fitness: 0.000000000.

4.8 Numerical Solution for the X Gate

Best candidate found:

$$(-1.5708, -3.14159, -8.20769 \cdot 10^{-10}, 6.28319, 2.98525 \cdot 10^{-15}).$$

For these values,

$$R_m = \begin{pmatrix} -4.9 \cdot 10^{-12} - 1.3 \cdot 10^{-6} i & 1.0 - 8.4 \cdot 10^{-7} i \\ 1.0 + 1.0 \cdot 10^{-6} i & -4.9 \cdot 10^{-12} - 1.3 \cdot 10^{-6} i \end{pmatrix}$$

Fitness: 0.000000000

4.9 Numerical Solution for the Y Gate

Best candidate found:

$$(-4.71239, -3.14159, -6.28319, 1.5708, -3.29535).$$

For these values,

$$R_m = \begin{pmatrix} 2.3 \cdot 10^{-6} - 9.7 \cdot 10^{-7} i & -4.7 \cdot 10^{-6} - 1.0i \\ -2.7 \cdot 10^{-6} + 1.0i & -2.3 \cdot 10^{-6} - 9.7 \cdot 10^{-7} i \end{pmatrix}$$

Fitness: 0.000000000.

4.10 Numerical Solution for the Z Gate

Best candidate found:

$$(1.5708, 3.14159, 3.14159, -1.92401, -3.4948).$$

For these values,

$$R_m = \begin{pmatrix} 1.0 - 2.7 \cdot 10^{-6} i & 1.9 \cdot 10^{-6} - 3.0 \cdot 10^{-7} i \\ 1.9 \cdot 10^{-6} + 3.0 \cdot 10^{-7} i & -1.0 - 4.7 \cdot 10^{-6} i \end{pmatrix}.$$

Fitness: 0.000000000.

4.11 Numerical Solution for the Identity Gate

Best candidate found:

$$(-6.28319, 6.28319, -6.28319, -6.28319, -6.28319).$$

For these values,

$$R_m = \begin{pmatrix} 1.0 - 4.69 \cdot 10^{-6} i & 0.0 + 0.0 i \\ 0.0 + 0.0 i & 1.0 - 4.69 \cdot 10^{-6} i \end{pmatrix}.$$

Fitness: 0.000000000.

From the above results, we realize that optimal values for θ, ϕ_1, ϕ_2, λ_1, and λ_2 were obtained. These optimal parameters enable us to implement any single-qubit gate (up to a global phase) with just two successive rotations when the two rotation axes are fixed in the xy plane.

Chapter 5

Conclusion

In this study, we have shown that single-qubit gates (up to a global phase) could be implemented with two successive rotations around arbitrary axes that are fixed in the xy plane. We constructively proved this by setting $\phi_2{=}\pi$ and ψ_2' $=0$. Obviously, this is not the only solution. A different choice of $\phi_1{=}\pi$ and $\psi_1'{=}0$ would lead to a another solution.

To summarize, we have demonstrated that efficient two-step implementations of single-qubit gates are possible when qubit rotation axes are tuned in a single plane (the xy plane was used in this work). In contrast, fixed-axis techniques (such as Euler angles method) require up to three sequential rotations. Our technique is readily applicable to superconducting qubits, especially to the transmon qubit. Veritably, any qubit implementation system that has at least partial control over the rotation axis could also utilize our two-step single qubit gate implementation technique. For instance, a singlet-triplet encoded qubit's [35] effective field is made up of a constant B_x component and a variable, positive B_z component. Since the resultant effective rotation axis occupies about half of the xz plane, efficient gating techniques like those discussed here are possible.

References

[1] D. E. Deutsch, "Quantum computational networks," *Proceedings of the Royal Society of London. A. Mathematical and Physical Sciences*, vol. 425, no. 1868, pp. 73–90, 1989.

[2] A. Barenco, C. H. Bennett, R. Cleve, D. P. DiVincenzo, N. Margolus, P. Shor, T. Sleator, J. A. Smolin, and H. Weinfurter, "Elementary gates for quantum computation," *Physical review A*, vol. 52, no. 5, p. 3457, 1995.

[3] M. Nielsen, "A & chuang, il quantum computation and information," 2000.

[4] M. A. Nielsen and I. Chuang, "Quantum computation and quantum information," 2011.

[5] G. Björk and J. Söderholm, "The dirac-notation in quantum optics," Technical Report, Department of Microelectronics and Information Technology ..., Tech. Rep., 2003.

[6] C. S. Calude, "Born rule and algorithmic randomness," 2019.

[7] B. Shim, G. Hays, R. Zgadzaj, T. Ditmire, and M. Downer, "Enhanced harmonic generation from expanding clusters," *Physical Review Letters*, vol. 98, no. 12, p. 123902, 2007.

[8] Y. Chen, M. Liu, J. Ulbricht, C.-H. Lin, J. Zhao, and A. S. Sakharov, "Finite size of electron in $e^+e^- \to \gamma + \gamma$ annihilation in differential cross section of centre-of-mass energies 55-207 gev," Tech. Rep., 2022.

[9] A. Montanaro, "Quantum algorithms: an overview," *npj Quantum Information*, vol. 2, no. 1, pp. 1–8, 2016.

[10] M. Kjaergaard, M. E. Schwartz, J. Braumüller, P. Krantz, J. I.-J. Wang, S. Gustavsson, and W. D. Oliver, "Superconducting qubits: Current state of play," *Annual Review of Condensed Matter Physics*, vol. 11, pp. 369–395, 2020.

[11] F. Arute, K. Arya, R. Babbush, D. Bacon, J. C. Bardin, R. Barends, R. Biswas, S. Boixo, F. G. Brandao, D. A. Buell *et al.*, "Quantum supremacy using a programmable superconducting processor," *Nature*, vol. 574, no. 7779, pp. 505–510, 2019.

[12] P. Krantz, M. Kjaergaard, F. Yan, T. P. Orlando, S. Gustavsson, and W. D. Oliver, "A quantum engineer's guide to superconducting qubits," *Applied Physics Reviews*, vol. 6, no. 2, p. 021318, 2019.

[13] W. D. Oliver and P. B. Welander, "Materials in superconducting quantum bits," *MRS bulletin*, vol. 38, no. 10, pp. 816–825, 2013.

[14] W. D. Oliver, Y. Yu, J. C. Lee, K. K. Berggren, L. S. Levitov, and T. P. Orlando, "Mach-zehnder interferometry in a strongly driven superconducting qubit," *Science*, vol. 310, no. 5754, pp. 1653–1657, 2005.

[15] J. Koch, M. Y. Terri, J. Gambetta, A. A. Houck, D. I. Schuster, J. Majer, A. Blais, M. H. Devoret, S. M. Girvin, and R. J. Schoelkopf, "Charge-insensitive qubit design derived from the cooper pair box," *Physical Review A*, vol. 76, no. 4, p. 042319, 2007.

[16] J. A. Schreier, A. A. Houck, J. Koch, D. I. Schuster, B. R. Johnson, J. M. Chow, J. M. Gambetta, J. Majer, L. Frunzio, M. H. Devoret *et al.*, "Suppressing charge noise decoherence in superconducting charge qubits," *Physical Review B*, vol. 77, no. 18, p. 180502, 2008.

[17] J. M. Fink, "Quantum nonlinearities in strong coupling circuit qed," Ph.D. dissertation, ETH Zurich, 2010.

[18] J. M. Gambetta, J. M. Chow, and M. Steffen, "Building logical qubits in a superconducting quantum computing system," *NPJ Quantum Information*, vol. 3, no. 1, pp. 1–7, 2017.

[19] R. Barends, J. Kelly, A. Megrant, D. Sank, E. Jeffrey, Y. Chen, Y. Yin, B. Chiaro, J. Mutus, C. Neill *et al.*, "Coherent josephson qubit suitable for scalable quantum integrated circuits," *Physical Review Letters*, vol. 111, no. 8, p. 080502, 2013.

[20] H. Paik, D. I. Schuster, L. S. Bishop, G. Kirchmair, G. Catelani, A. P. Sears, B. Johnson, M. Reagor, L. Frunzio, L. I. Glazman *et al.*, "Observation of high coherence in josephson junction qubits measured in a three-dimensional circuit qed architecture," *Physical Review Letters*, vol. 107, no. 24, p. 240501, 2011.

[21] Y.-P. Shim, J. Fei, S. Oh, X. Hu, and M. Friesen, "Single-qubit gates in two steps with rotation axes in a single plane," *arXiv preprint arXiv:1303.0297*, 2013.

[22] D. P. DiVincenzo, "Two-bit gates are universal for quantum computation," *Phys. Rev. A*, vol. 51, no. 2, p. 1015, 1995.

[23] M. Nielsen, "A & chuang, il quantum computation and information," 2000.

[24] Y.-P. Shim, J. Fei, S. Oh, X. Hu, and M. Friesen, "Single-qubit gates in two steps with rotation axes in a single plane," *arXiv preprint arXiv:1303.0297*, 2013.

[25] J. R. Petta, A. C. Johnson, J. M. Taylor, E. A. Laird, A. Yacoby, M. D. Lukin, C. M. Marcus, M. P. Hanson, and A. C. Gossard, "Coherent manipulation of coupled electron spins in semiconductor quantum dots," *Science*, vol. 309, no. 5744, pp. 2180–2184, 2005.

[26] X. Wang, L. S. Bishop, J. Kestner, E. Barnes, K. Sun, and S. Das Sarma, "Composite pulses for robust universal control of singlet–triplet qubits," *Nat. Commun.*, vol. 3, no. 1, pp. 1–7, 2012.

[27] J. P. Kestner, X. Wang, L. S. Bishop, E. Barnes, and S. D. Sarma, "Noise-resistant control for a spin qubit array," *Phys. Rev. Lett.*, vol. 110, no. 14, p. 140502, 2013.

[28] P. M. Pardalos and H. E. Romeijn, *Handbook of Global Optimization: Volume 2*. Springer Science & Business Media, 2013, vol. 62.

[29] J. Nocedal and S. J. Wright, *Numerical optimization*. Springer, 1999.

[30] M. S. Daoud, M. Shehab, H. M. Al-Mimi, L. Abualigah, R. A. Zitar, and M. K. Y. Shambour, "Gradient-based optimizer (gbo): A review, theory, variants, and applications," *Archives of Computational Methods in Engineering*, pp. 1–19, 2022.

[31] "Blackboxoptim.jl."

[32] S. Boyd, S. P. Boyd, and L. Vandenberghe, *Convex optimization*. Cambridge university press, 2004.

[33] C. A. Floudas and C. E. Gounaris, "A review of recent advances in global optimization," *Journal of Global Optimization*, vol. 45, no. 1, pp. 3–38, 2009.

[34] F. Jia and D. Lichti, "A comparison of simulated annealing, genetic algorithm and particle swarm optimization in optimal first-order design of indoor tls networks." *ISPRS Annals of Photogrammetry, Remote Sensing & Spatial Information Sciences*, vol. 4, 2017.

[35] J. R. Petta, A. C. Johnson, J. M. Taylor, E. A. Laird, A. Yacoby, M. D. Lukin, C. M. Marcus, M. P. Hanson, and A. C. Gossard, "Coherent manipulation of coupled electron spins in semiconductor quantum dots," *Science*, vol. 309, no. 5744, pp. 2180–2184, 2005.

Vita

Edward Takyi graduated in 2018 from University of Cape Coast, Ghana, and got his Bachelor of Science degree in Engineering Physics. After graduation, he worked as a Laboratory Assistant at Morgan International Community School. He came to the United States in January 2021 for his Master's in Physics at UTEP and he has been conducting his research under the supervision of Dr. Yun-Pil Shim.

His current research interest is in studying Two-Step Single Qubit Gates for Superconducting Qubits.